Available online at www.sciencedirect.com
ScienceDirect
Ceramics International 40 (2014) 13537–13541
CERAMICS INTERNATIONAL
www.elsevier.com/locate/ceramint

Gas pressure sintering of BN/Si_3N_4 wave-transparent material with Y_2O_3–MgO nanopowders addition

Yujun Zhao[a,b], Yujun Zhang[a,b,*], Hongyu Gong[a,b], Haibin Sun[a,b], Qisong Li[a,b]

[a]Key Laboratory for Liquid-Solid Structural Evolution & Processing of Materials of Ministry of Education, Shandong University, Jinan 250061, P.R. China
[b]Key Laboratory of Special Functional Aggregated Materials, Ministry of Education, Shandong University, Jinan 250061, P.R. China

Received 6 March 2014; received in revised form 7 May 2014; accepted 8 May 2014
Available online 29 May 2014

Abstract

BN/Si_3N_4 ceramics performed as wave-transparent material in spacecraft were fabricated with boron nitride powders, silicon nitride powders and Y_2O_3–MgO nanopowders by gas pressure sintering at 1700 °C under 6 MPa in N_2 atmosphere. The effects of Y_2O_3–MgO nanopowders on densification, phase evolution, microstructure and mechanical properties of BN/Si_3N_4 material were investigated. The addition of Y_2O_3–MgO nanopowders was found beneficial to the mechanical properties of BN/Si_3N_4 composites. The BN/Si_3N_4 ceramics with 8 wt% Y_2O_3–MgO nanopowders showed a relative density of 80.2%, combining a fracture toughness of 4.6 MPa m$^{1/2}$ with an acceptable flexural strength of 396.5 MPa.

Keywords: C. Mechanical properties; BN/Si_3N_4 wave-transparent material; Gas pressure sintering; Y_2O_3–MgO nanopowders

1. Introduction

Si_3N_4 was one of the most promising ceramics for the application of microwave-transparent materials which protected the spacecraft from the influences of harsh environment [1,2] due to its high mechanical strength, good thermal shock resistance and excellent rain erosion resistance [3–5]. However, the relatively high dielectric constant and dielectric loss tangent limited its wider application in spaceflight [6,7]. In order to improve dielectric properties of Si_3N_4 ceramics, BN nanoparticles with low dielectric constant and low thermal expansion coefficient were introduced into Si_3N_4 matrix to fabricate BN/Si_3N_4 composites by gas pressure sintering [8,9]. Therefore BN/Si_3N_4 composites have low dielectric constant and outstanding mechanical properties.

However, a sintered body with high density of BN/Si_3N_4 composites was difficult to be obtained due to strong covalent bonds between Si–N and B–N [10]. Some metal oxides such as MgO, Al_2O_3, Y_2O_3 and Re_2O_3 have been used as sintering additives for the densification of Si_3N_4 [11–14]. The liquid formed via the chemical reactions between the additives and SiO_2 in Si_3N_4 could enhance the diffusivity of atoms to reduce the sintering temperature. Finally we can fabricate the most promising BN/Si_3N_4 materials because of their excellent strength and toughness at elevated temperatures, good thermal shock resistance and dielectric properties, and low coefficient of thermal expansion [15–16].

Y_2O_3 has been a promising sintering additive for both pressureless and gas-pressure sintered Si_3N_4 [11,12,17–20]. Although the microstructure and mechanical properties of sintered Si_3N_4 containing Y_2O_3, Re_2O_3, Al_2O_3, MgO have been previously reported [11–14], the effects of Y_2O_3–MgO nanopowders on the developed microstructure and elevated-temperature properties need further research. Nevertheless, few reports were devoted to the effect of Y_2O_3–MgO composite nanopowders or its precursors as sintering aids over the mechanical and microstructure of BN/Si_3N_4 wave-transparent material. So in the present work, the effect of Y_2O_3–MgO composite nanopowders on the densification and mechanical

*Corresponding author at: Key Laboratory of Special Functional Aggregated Materials, Ministry of Education, Shandong University, Jinan 250061, P.R. China. Tel./fax: +86 531 88399760.
E-mail address: yujunzhangcn@sud.edu.cn (Y. Zhang).

http://dx.doi.org/10.1016/j.ceramint.2014.05.054

properties of BN/Si_3N_4 wave-transparent material was investigated. In addition, microstructural development and phase evolution of sintered samples were investigated with the help of SEM and XRD.

2. Experimental procedures

Tα-Si_3N_4 powders (α-Si_3N_4 > 93%, D50 < 0.5 μm; UNISCERA, Beijing, China) and BN nanoparticles (purity > 99.5 wt%, D50 < 100 nm; NNT CO., Taiwan, China) were used as starting materials. The additives used in this work were Y_2O_3 (Hang Zhou Wan Jing New Material Co., Ltd. P.R. China) with the average grain size of 50 nm and 100 nm and MgO (Hang Zhou Wan Jing New Material Co., Ltd. P.R. China) with the average grain size of 50 nm. Y_2O_3–MgO composites were prepared in our laboratory with particle size of less than 80 nm via an esterification sol–gel processing [21] using the following reagents: magnesium nitrate ($Mg(NO_3)_2 \cdot 6H_2O$) (AR, Sinopharm Chemical Reagent Co., Ltd), yttrium nitrate ($Y(NO_3)_3 \cdot 6H_2O$) (AR, Sinopharm Chemical Reagent Co., Ltd), citric acid (AR, Sinopharm Chemical Reagent Co., Ltd) and ethylene glycol (AR, Sinopharm Chemical Reagent Co., Ltd). The XRD pattern and SEM micrographs of the Y_2O_3–MgO nanopowders are shown in Fig. 1. The results from X-ray diffraction (Fig. 1(a)) indicated that Y_2O_3–MgO nanopowder was a two-phase material consisting of cubic Y_2O_3 and cubic MgO phase. The average particle size of the powders was normally below 80 nm (Fig. 1(b)). The BN nanoparticles were previously washed with methanol to remove little B_2O_3 contamination. The compositions of different samples are referred in Table 1.

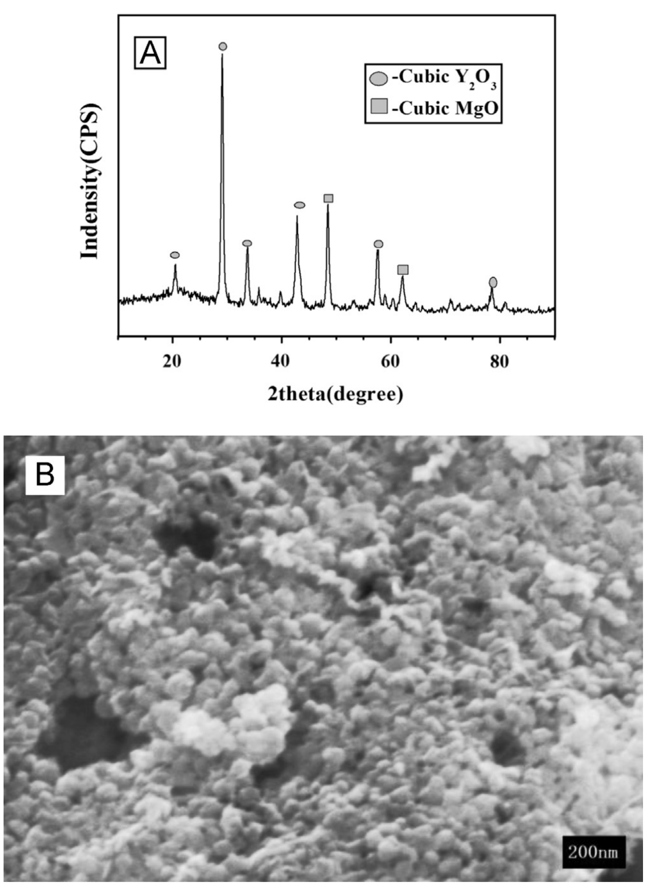

Fig. 1. XRD pattern and SEM micrographs of Y_2O_3–MgO nanopowders.

100 nm-Y_2O_3 + 50 nm-MgO,50 nm-Y_2O_3 + 50 nm-MgO, Y_2O_3–MgO precursor and Y_2O_3–MgO nanopowders were added to the starting powders as the sintering aids. The starting powders and sintering aids were mixed in anhydrous ethanol by a vertical ball mill, followed by drying at 60 °C for 24 h under vacuum. The mixture was then passed through 200 μm vibrating sieve. This precursor powder was compacted by uniaxial processing to produce square green body with unilateral length of 55 mm. The green body was molded by an isostatic pressing method with rubber mold under 120 MPa.

The BN/Si_3N_4 green body was sintered in BN-coated graphite dyes at 1700 °C for 120 min under a steady pressure of 6 MPa in N_2 atmosphere. The compacted samples were heated to 1700 °C in N_2 atmosphere with a heating/cooling rate of 5 °C/min in gas pressure sintering furnace. The apparent porosity was determined by Archimedes' method using deionized water as a medium. The bending strength was measured by three-point bending test and the fracture toughness was determined by a single edge pre-cracked beam method. The fracture surface of specimens was coated with Au for SEM (Hitachi S-520, Hitachi Ltd., Tokyo, Japan) observation.

3. Results and discussion

3.1. Densification behavior

Fig. 2 plots the apparent porosity and relative density of the BN/Si_3N_4 ceramics with different sintering aids such as 100 nm-Y_2O_3 + 50 nm-MgO, 50 nm-Y_2O_3 + 50 nm-MgO, Y_2O_3–MgO precursor and Y_2O_3–MgO nanopowders. The addition of the sintering aids decreases the apparent porosity and therefore increases the relative density of BN/Si_3N_4 ceramics. Compared with the other three sintering aids, Y_2O_3–MgO composite nanopowders are more beneficial to the densification of BN/Si_3N_4 ceramics and the relative density and apparent porosity reach 80.2% and 9.6%

Table 1
Composition of samples.

Sample's label	Composition of samples	Amount of Y_2O_3/MgO composite additives (wt%)
SBY100M50	Si_3N_4 + 10 wt%BN + 100 nm-Y_2O_3 + 50 nm-MgO	8
SBY50M50	Si_3N_4 + 10 wt%BN + 50 nm-Y_2O_3 + 50 nm-MgO	8
SBY1M1	Si_3N_4 + 10 wt%BN + Y_2O_3–MgO precursor	8
SBY0M0	Si_3N_4 + 10 wt%BN + Y_2O_3–MgO nanopowders	8

The molar ratio of the Y_2O_3/MgO was fixed at Y_2O_3:MgO = 1:1

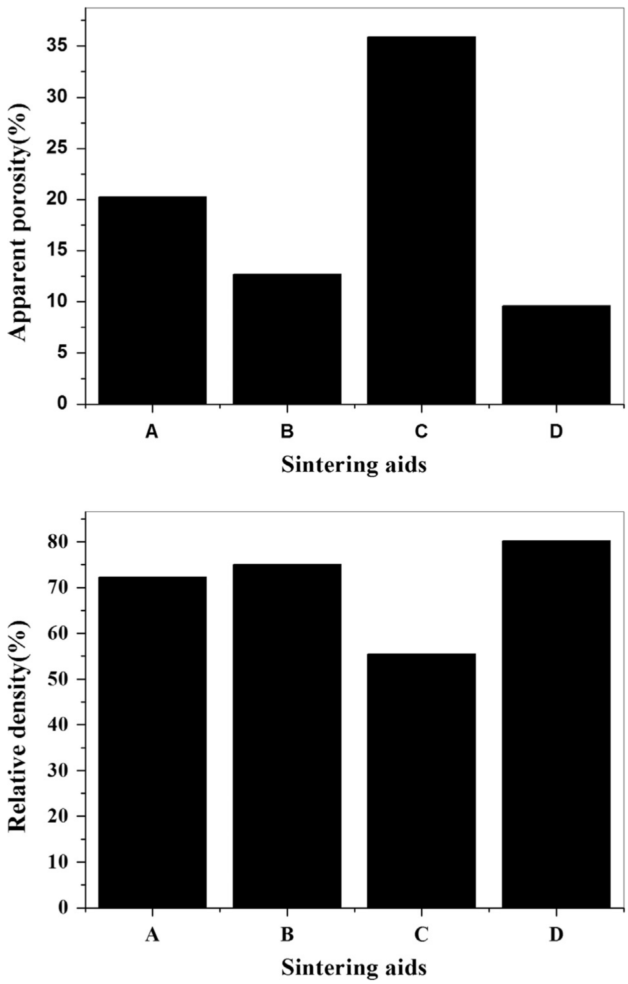

Fig. 2. Influence of different sintering aids on the apparent porosity and relative density of BN/Si_3N_4 wave-transparent material. A: SBY100M50; B: SBY50M50; C: SBY1M1; D: SBY0M0. (A) Histogram of 100 nm-Y_2O_3 + 50 nm-MgO on the apparent porosity and density of BN/Si_3N_4 wave-transparent material. (B) Histogram of 50 nm-Y_2O_3 + 50 nm-MgO on the apparent porosity and density of BN/Si_3N_4 wave-transparent material. (C) Histogram of Y_2O_3–MgO precursor on the apparent porosity and density of BN/Si_3N_4 wave-transparent material. (D) Histogram of Y_2O_3–MgO nanopowders on the apparent porosity and density of BN/Si_3N_4 wave-transparent material.

respectively. Owing to the formation of ample liquid phase at lower temperature which assists mass transport and rearrangement [22], the densification of BN/Si_3N_4 ceramics proceeds quickly with the addition of Y_2O_3–MgO composite nanopowders [23–25], whereas the BN/Si_3N_4 material using Y_2O_3–MgO precursor as sintering aids shows the minimal relative density and maximum apparent porosity, reaching 55.5% and 35.88% respectively. The possible reason is that big pores appear with the decomposition or evaporation of the organic chemicals in Y_2O_3–MgO precursor in the sintering process.

3.2. Mechanical properties

Fig. 3 presents the mechanical properties of BN/Si_3N_4 ceramics with different sintering aids. It can be seen that the BN/Si_3N_4 material with the sintering aid of Y_2O_3–MgO nanopowders exhibits the maximum bending strength and fracture toughness, reaching 396.5 MPa and 4.6 MPa $m^{1/2}$ respectively, whereas the BN/Si_3N_4 material using Y_2O_3–MgO precursor as sintering aids shows the minimal bending strength and fracture toughness, reaching 137 MPa and 2.73 MPa $m^{1/2}$ respectively. The possible reason is that big pores appear with the decomposition or evaporation of the organic chemicals in the Y_2O_3–MgO precursor in the sintering process. Compared with SBY100M50, SBY50M50, SBY1M1 and SBY0M0 are more effective in improving the mechanical properties, especially the fracture toughness of BN/Si_3N_4 composites. The possible reason is that Y_2O_3 promotes the formation of rod-like Si_3N_4 particles and MgO promotes the densification of BN/Si_3N_4 wave-transparent material [26]. In addition, compared with the other three sintering aids, the higher temperature activity and homogeneity of Y_2O_3–MgO nanopowders are more beneficial to the mechanical properties and fracture toughness [27].

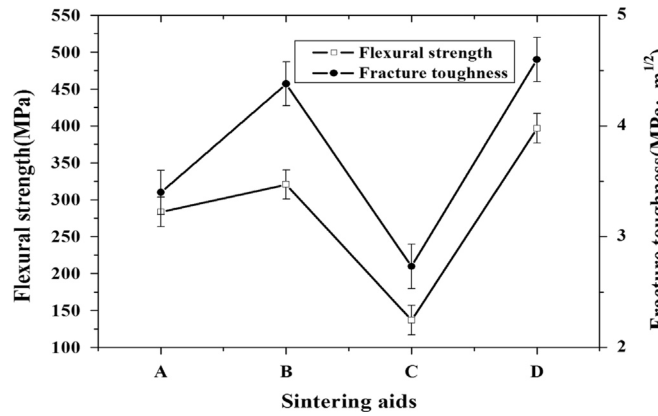

Fig. 3. Influence of different sintering aids on the mechanical properties of BN/Si_3N_4 wave-transparent material. A: SBY100M50; B: SBY50M50; C: SBY1M1. (A) Curve of 100 nm-Y_2O_3 + 50 nm-MgO on the mechanical properties of BN/Si_3N_4 wave-transparent material. (B) Curve of 50 nm-Y_2O_3 + 50 nm-MgO on the mechanical properties of BN/Si_3N_4 wave-transparent material. (C) Curve of Y_2O_3–MgO precursor on the mechanical properties of BN/Si_3N_4 wave-transparent material. (D) Curve of Y_2O_3–MgO nanopowders on the mechanical properties of BN/Si_3N_4 wave-transparent material.

3.3. Phase evolution

Fig. 4 shows the XRD pattern of BN/Si_3N_4 wave-transparent materials with different sintering aids. The XRD pattern shows that the main crystal phase of the composites is β-Si_3N_4, and no α-Si_3N_4 is detected. The existence of Si_2N_2O can be explained by the following reaction which occurs during the sintering process when the temperature reaches 1600 °C [28]:

$$2Si_3N_4(s) + 1.5O_2(g) \rightarrow 3Si_2N_2O(s) + N_2(g) \quad (1)$$

When the temperature is higher than 1650 °C, the following reaction occurs and the amount of Si_2N_2O decreases [28]:

$$2Si_2N_2O(s) \rightarrow Si_3N_4(s) + SiO(g) + 0.5O_2(g) \quad (2)$$

Based on thermodynamic calculations, $MgSiO_3$ is formed readily by a reaction between MgO and SiO_2 at α-Si_3N_4 surface as a silicate liquid phase during sintering and then transformed into its glassy phase after cooling down [29]. Maybe it is the reason why no diffraction peaks of MgO are observed. These results supported the α-Si_3N_4–β-Si_3N_4 transformation with the help of sintering additives after the solution of α-Si_3N_4 fine grains and the subsequent reprecipitation as β-Si_3N_4 phase [30]. Distinct reflections of h-BN and Y_2O_3 are observed in the XRD pattern at 26.5° and 31°(2θ).

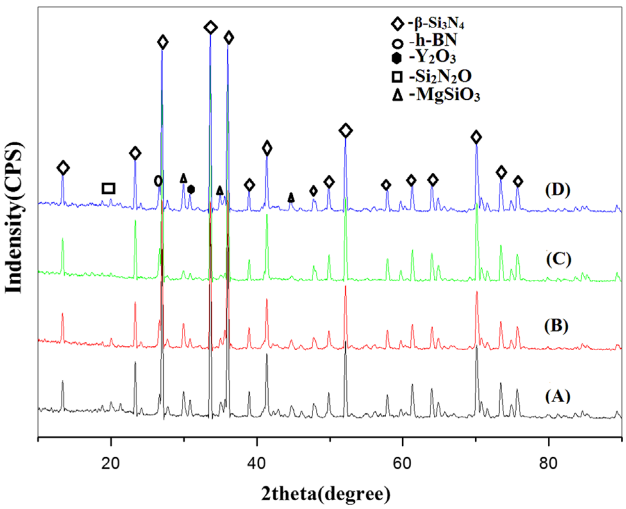

Fig. 4. Influence of different sintering aids on phase evolution of BN/Si_3N_4 wave-transparent material. A: SBY100M50; B: SBY50M50; C: SBY1M1; D: SBY0M0. (A) XRD pattern of 100 nm-Y_2O_3+50 nm-MgO on phase evolution of BN/Si_3N_4 wave-transparent material. (B) XRD pattern of 50 nm-Y_2O_3+50 nm-MgO on phase evolution of BN/Si_3N_4 wave-transparent material. (C) XRD pattern of Y_2O_3–MgO precursor on phase evolution of BN/Si_3N_4 wave-transparent material. (D) XRD pattern of Y_2O_3–MgO nanopowders on Phase evolution of BN/Si_3N_4 wave-transparent material.

3.4. Microstructure

The fracture microstructures of BN/Si_3N_4 wave-transparent composites with different sintering aids can be seen in Fig. 5. It can be clearly seen that more amount of rod-like β-Si_3N_4 particles with higher mean aspect ratio and narrower grain size distribution form in the BN/Si_3N_4 composites with Y_2O_3–MgO nanopowders as sintering aids than the other three sintering aids (Fig. 5(A)–(D)). It is possibly due to the fact that Y_2O_3–MgO nanopowders are formed in molecular level and have higher activation energy and homogeneity than Y_2O_3 or MgO powder [27]. The high temperature activity of Y_2O_3–MgO nanopowders may improve the α–β transformation of Si_3N_4 at 1700 °C. The rod-like β phase grains lead to improvement in the fracture toughness of the material, and the toughening mechanism is similar to that in whisker reinforced composite materials, i.e. grain bridging by elongated grains and grain pullout [31].

4. Conclusions

The sintering aids promoted the densification of BN/Si_3N_4 wave-transparent materials and increased their mechanical properties. The BN/Si_3N_4 composites using Y_2O_3–MgO nanopowders as sintering aids exhibited the maximum densification, bending strength and fracture toughness, reaching 2.75 g/cm^3, 396.5 MPa and 4.6 MPa m$^{1/2}$ respectively. In addition, when the sintering aids were added to the BN/Si_3N_4 wave-transparent material, all α-Si_3N_4 particles transformed to rod-like β-Si_3N_4 after sintering. When using Y_2O_3–MgO nanopowders as sintering aids, more elongated

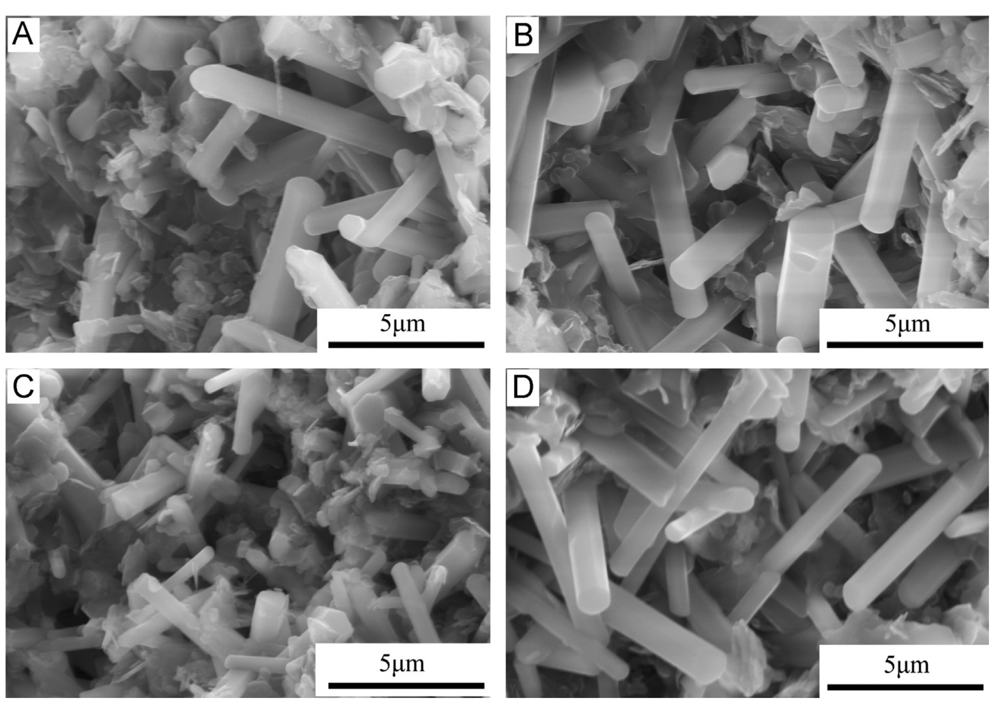

Fig. 5. SEM micrograph of BN/Si_3N_4 wave-transparent material with different additives. A: SBY100M50; B: SBY50M50; C: SBY1M1; D: SBY0M0. (A) SEM micrograph of 100 nm-Y_2O_3+50 nm-MgO on the microstructures of BN/Si_3N_4 wave-transparent material. (B) SEM micrograph of 50 nm-Y_2O_3+50 nm-MgO on the microstructures of BN/Si_3N_4 wave-transparent material. (C) SEM micrograph of Y_2O_3–MgO precursor on the microstructures of BN/Si_3N_4 wave-transparent material. (D) SEM micrograph of Y_2O_3–MgO nanopowders on the microstructures of BN/Si_3N_4 wave-transparent material.

and interlocked rod-like β-Si_3N_4 grains and higher mean aspect ratio formed in BN/Si_3N_4 wave-transparent material, which led to the improvement of mechanical properties of BN/Si_3N_4 wave-transparent materials.

References

[1] S. Ding, Y.P. Zeng, D. Jiang, Oxidation bonding of porous silicon nitride ceramics with high strength and low dielectric constant, Mater. Lett. 61 (2007) 2277–2280.

[2] G. Qi, C. Zhang, H. Hu, High strength three-dimensional silica fiber reinforced silicon nitride-based composites via poly hydridomethylsilazane pyrolysis, Ceram. Int. 3 (2007) 891–894.

[3] J. Barta, M. Manela, R. Fischer, Si_3N_4 and Si_2N_2O for high performance randomes, Mater. Sci. Eng. 71 (1985) 265–272.

[4] F.L. Riley, et al., Silicon nitride and related materials, J. Am. Ceram. Soc. 83 (2000) 245–265.

[5] A. Ziegler, J.C Idrobo, M.K. Cinibulk, C. Kisielowski, N.D. Browning, R.O. Ritchie, Interface structure and atomic bonding characteristics in silicon nitride ceramics, Science 306 (2004) 1768–1770.

[6] Y. Liu, L. Cheng, L. Zhang, Y. Xu, Fabrication and characterization of $SiO_{2(f)}$/Si_3N_4 composites, J. Univ. Sci. Technol. Beijing 14 (2007) 454–459.

[7] X. Li, X. Tin, L. Cheng, Y. Qi, Mechanical and dielectric properties of porous Si_3N_4–SiO_2 composite ceramics, Mater. Sci. Eng. 500 (2009) 63–69.

[8] R.G. Wang, W. Pan, M.N. Jiang, J. Chen, Y. Luo, Investigation of the physical and mechanical properties of hot-pressed machinable Si_3N_4/h-BN composites and FGM, Mater. Sci. Eng. 90 (2002) 261–268.

[9] P. Rendtel, A. Rendtel, H. Huber, Mechanical properties of gas pressure sintered Si_3N_4/SiC nanocomposites, J. Eur. Ceram. Soc. 22 (2002) 2061–2070.

[10] C.M. Wang, X.Q. Pan, M. Ruhle, F.L. Riley, M. Mitomo, Review: silicon nitride crystal structure and observations of lattice defects, J. Mater. Sci. 31 (1996) 5281–5298.

[11] N. Hirosaki, Y. Okamoto, Y. Akimune, M. Mitomo, Sintering of Y_2O_3–Al_2O_3-doped β-Si_3N_4 powder and mechanical properties of sintered materials, J. Ceram. Soc. Jpn. 102 (1994) 791–795.

[12] D.R. Clarke, G. Thomas, Microstructure of Y_2O_3 fluxed hot-pressed silicon nitride, J. Am. Ceram. Soc. 61 (3–4) (1978) 114–118.

[13] Y. Goto, G. Thomas, Microstructure of silicon nitride ceramics sintered with rare-earth oxide, Acta Metall. Mater. 43 (3) (1995) 923–930.

[14] K.S. Mazdiyasni, C.M. Cooke, Consolidation, microstructure, and mechanical properties of Si_3N_4 doped with rare-earth oxides, J. Am. Ceram. Soc. 57 (12) (1974) 536–537.

[15] O.L. Krivanek, T.M. Shaw, G. Thomas, The microstructure and distribution of impurities in hot-pressed and sintered silicon nitride, J. Am. Ceram. Soc. 62 (11–12) (1979) 585–590.

[16] D.R. Clarke, et al., On the equilibrium thickness of intergranular glass phases in ceramic materials, J. Am. Ceram. Soc. 70 (1) (1987) 15–22.

[17] A. Tsuge, K. Nishida, M. Komatsu, Effect of crystallizing the grain-boundary glass phase on the high-temperature strength of hot-pressed Si_3N_4 containing Y_2O_3, J. Am. Ceram. Soc. 58 (7–8) (1975) 323–326.

[18] M.K. Cinibulk, G. Thomas, S.M. Johnson, Fabrication and secondary-phase crystallization of rare-earth disilicate–silicon nitride ceramics, J. Am. Ceram. Soc. 75 (8) (1992) 2037–2043.

[19] M.K. Cinibulk, G. Thomas, S.M. Johnson, Strength and creep behavior of rare-earth disilicate silicon nitride ceramics, J. Am. Ceram. Soc. 75 (8) (1992) 2050–2055.

[20] D.M. Mieskowski, W.A. Sanders, Oxidation of silicon nitride sintered with rare-earth oxide additions, J. Am. Ceram. Soc. 68 (7) (1985) 160–163.

[21] Chun-Hu Chen, Jacquelynn K.M. Garofano, et al., A foaming esterification sol–gel route for the synthesis of magnesia–yttria nanocomposites, J. Am. Ceram. Soc. 94 (2) (2011) 367–371.

[22] T. Nishimura, M. Mitomo, H. Suematsu, High temperature strength of silicon nitride ceramics with ytterbium silicon oxynitride, J. Mater. Res. 12 (1) (1997) 203–209.

[23] Y. Goto, G. Thomas, Phase transformation and microstructural changes of Si_3N_4 during sintering, J. Mater. Sci. 30 (1995) 2194–2200.

[24] H.-H. Lu, J.-L. Huang, Microstructure in silicon nitride containing β-phase seeding, Part 1, J. Mater. Res. 14 (7) (1999) 2966–2973.

[25] V.K. Sarin, et al., On the α-to-β phase transformation in silicon nitride, Mater. Sci. Eng. A 105/106 (1988) 151–159.

[26] Kevin P. Plucknett, Mervin Quinlan, Liliana Garrido, Luis Genova, Microstructural development in porous β-Si_3N_4 ceramics prepared with low volume RE_2O_3–Mg–(CaO) additions (RE = La, Nd, Y, Yb), Mater. Sci. Eng. A 489 (2008) 337–350.

[27] A.J. Pzik, D.F. Carroll, C.J. Hwang, P.F. Becher, M. Mitomo, Silicon nitride ceramics: scientific and technological issues, Mater. Res. Soc. 287 (1993) 411–416.

[28] Chunyan Tian, Ning Liu, Maohua Lu, Effect of WC on microstructure and mechanical properties of silicon nitride nano-composites, J. Mater. Process. Technol. 205 (2008) 411–418.

[29] Alfian Noviyanto, Dang-Hyok Yoon, Metal oxide additives for the sintering of silicon carbide:reactivity and densification, Curr. Appl. Phys. 13 (2013) 287–292.

[30] D.D. Lee, S.J.L. Kang, D.N. Yoon, Mechanism of grain growth and α-to-β transformation during liquid phase sintering of β-sialon, J. Am. Ceram. Soc. 71 (9) (1988) 803–806.

[31] D.L. Zhao, Y.J. Zhang, H.Y. Gong, L.F. Nie, L. Zhao, Effects of sintering aids on mechanical and dielectric properties of Si_3N_4 ceramics, Mater. Res. Innov. 14 (2010) 338–341.